Rapid analysis of S-Adenosylmethionine (SAM) and S-Adenosylhomocysteine (SAH) isotopologues in stable isotope-resolved metabolomics (SIRM) using direct infusion nanoelectrospray ultra-high-resolution Fourier transform mass spectrometry (DI-nESI-UHR-FTMS)

Joon Seon Yang, **Teresa W.M. Fan**, **Jason A. Brandon**, **Andrew N. Lane**, **Richard M. Higashi**

Center for Environmental and Systems Biochemistry (CESB), Markey Cancer Center, and Department of Toxicology and Cancer Biology, University of Kentucky, USA
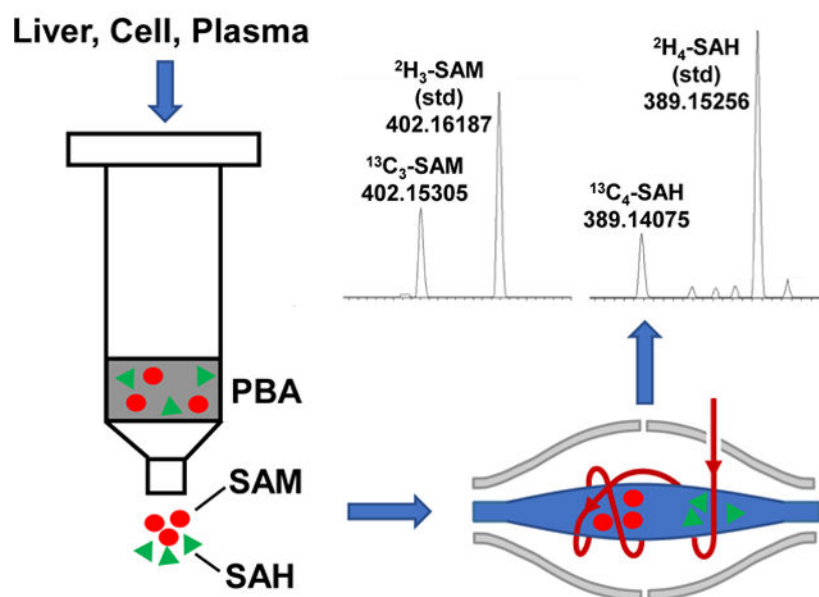
Abstract

S-Adenosylmethionine (SAM) and S-adenosylhomocysteine (SAH) are important metabolites in the one-carbon cycle that modulates cellular methylation required for proliferation and epigenetic regulation. Their concentrations, synthesis, and turnover are difficult to determine conveniently and reliably. We have developed such a method by coupling a simple and rapid purification scheme that efficiently captures both compounds, with high sensitivity, sample throughput direct infusion nanoelectrospray ultra-high-resolution Fourier transform mass spectrometry (DI-nESI-UHR-FTMS). This method is compatible with Stable Isotope-Resolved Metabolomic (SIRM) analysis of numerous other metabolites. The limits of detection for both SAM and SAH were < 1 nM, and the linearity range was up to 1000 nM. The method was first illustrated for SAM/SAH analysis of mouse livers, and lung adenocarcinoma A549 cells. We then applied the method to track $^{13}C_1$-CH_3-Met incorporation into SAM and $^{13}C_6$-glucose transformation into SAM and SAH via de novo synthesis. We further used the method to show the distinct effects on A549 and H1299 cells with treatment of anti-cancer methylseleninic acid (MSA), selenite, and selenomethionine, notably SAM depletion and increased SAM to SAH ratio by MSA, which implicates altered epigenetic regulation.

Graphical Abstract

Correspondence to: Teresa W-M. Fan teresa.fan@uky.edu Or Richard M. Higashi rick.higashi@uky.edu, Center for Environmental and Systems Biochemistry, 789 S. Limestone St., Lexington, KY 40536, USA, Ph: 859-218-1028.

1. Introduction

Methionine is a sulfur-containing essential amino acid participating in the one-carbon metabolism (Figure 1), which continuously interconvert S-adenosylmethionine (SAM) and methionine [1–3]. The cycle begins with the generation of S-adenosylmethionine (SAM) from methionine, utilizing ATP as a co-substrate via methionine adenosyltransferase (MAT) [4–6]. SAM is biologically important in that it is a universal methyl donor in a wide range of methylation reactions and is the second most common cofactor after ATP in various enzymatic reactions [7]. The methyl group on the sulfur atom of SAM can be transferred to various substrates including DNA, RNA, proteins, glycine, polyamines, and phosphatidylethanolamine (PE) through a transmethylation reaction [3, 8]. SAM is thereby irreversibly converted to S-adenosylhomocysteine (SAH). SAH is then hydrolyzed to adenosine plus homocysteine by *S*-adenosylhomocysteine hydrolase. Homocysteine is either further converted to cysteine via the transsulfuration pathway or is remethylated by methionine synthase using 5-methyl-tetrahydrofolate (5-methyl-THF). This recycling of homocysteine is critical to regenerating methionine and maintaining the transmethylation cycles [9, 10].

The ratio of SAM to SAH, which is called "methylation index", is physiologically important because it controls most biological methylation reactions including epigenetic DNA and histone methylation, which is central to regulating gene expression in both normal and disease states including cancers [11–13]. Increased SAM to SAH ratios have been associated with many diseases such as cardiovascular diseases, renal failure and liver diseases, where

protein methylation is altered. The SAM to SAH ratio in human serum has also been reported to be a sensitive indicator of atherosclerosis [10, 11, 14–17]. Therefore, by governing the methylation of various biomolecules, the ratio of SAM to SAH is closely linked to human pathophysiological conditions.

As SAH is typically found at a much lower level than SAM [18], and the ratio changes under pathological conditions, it is therefore important to measure both SAM and SAH accurately. Several methods have been developed for determining this ratio such as the fluorescence polarization immunoassay, colorimetric enzymatic methods [19–21], or liquid chromatography coupled with tandem mass spectrometry (LC-MS/MS) based analysis [22–26]. The former two methods lack selectivity or have poor reproducibility, while the LC-MS/MS method coupled with the use of commercially available stable isotope-enriched standards is preferred due to its high selectivity, sensitivity, and accuracy as well as molecular structural determination, which makes it compatible with SIRM applications. However, the LC-MS/MS method is time-consuming, which makes it less compatible with high throughput applications and data analysis. A fast and robust sample preparation method coupled with direct infusion nanoelectrospray ultra-high-resolution Fourier transform mass spectrometry (DI-nESI-UHR-FTMS) is an attractive alternative method as high-resolution and mass accuracy data are acquired without physical separation for high-speed and robust metabolite analysis [27, 28].

Moreover, the ability of DI-nESI-UHR-FTMS to accurately measure isotopically enriched mass isotopologues makes it particularly suited for stable isotope-resolved metabolomics (SIRM) applications. SIRM is a powerful and rigorous approach for mapping metabolic networks in cells or tissues to uncover metabolic dysregulations induced by disease development or stressor treatments. It has been applied to most biosystems ranging from microbial systems to human subjects [29–31]. As SIRM relies on untargeted MS[1] to obtain whole-metabolite isotopic incorporation, it depends on both accurate mass and ultra-high mass resolution to quantify as many metabolite isotopologues as possible. This, in turn, greatly benefits from long (many minutes) data acquisition times afforded by direct infusion than by LC (a few seconds). UHR-FTMS also enables analysis of multiple tracer atoms in the same or different metabolites for multiplexed SIRM applications [22, 32].

There have been a few studies that utilized direct infusion mass spectrometry to measure SAM and SAH [33], but none have been applied to analyzing isotope labeled SAM and SAH resulting from metabolism. The latter applications have a much higher sensitivity requirement due to the distribution of mass signals into various isotopologues. In this study, we describe a simple, rapid, and highly sensitive method for SAM and SAH analysis for cells and tissues by coupling phenylboronic acid (PBA) affinity capture with DI-nESI-UHR-FTMS. The method is fully compatible with comprehensive profiling of metabolites using methods such as ion chromatography-UHR-FTMS. We have applied this method to SAM/SAH analysis of mouse livers and lung adenocarcinoma A549 or H1299 cells. We further used the method to track ^{13}C incorporation into SAM and SAH in A549 cells treated with $^{13}C_1$-CH_3-Methionine or $^{13}C_6$-glucose, and to probe the distinct effect of anti-cancer selenium treatments in A549 and H1299 cells.

2. Experimental

2.1 Materials and reagents

HPLC grade ammonium acetate, acetonitrile, methanol, formic acid, acetic acid, 28% ammonia solution, and chloroform were purchased from Sigma Aldrich (St. Louis, MO, USA). Bond-Elut SPE phenylboronic acid (PBA) columns were ordered from Agilent Technologies (Santa Clara, CA, USA). Unlabeled SAM and SAH standards were obtained from Fisher Scientific (Pittsburgh, PA, USA). $^2H_3$-SAM was purchased from Medical Isotopes, Inc. (Pelham, NH, USA) and $^2H_4$-SAH was obtained from Cayman Chemical (Ann Arbor, MI, USA).

2.2 Cell culturing, treatment, and extraction

A549 or H1299 human lung adenocarcinoma cells (American Type Culture Collection (Rockville, MD)) were cultured in DMEM (pH 7.4) supplemented with 10% v/v fetal bovine serum, 3.7 g L^{-1} sodium bicarbonate, 0.2% Glucose, 2 mM Glutamine and 1x Penicillin-Streptomycin (complete DMEM) and maintained at 37 °C in a 5% CO_2 humidified atmosphere. Cells were lifted using TripLE (GIBCO, Life technologies, NY) and reseeded at a density of 8.7×10^5 cells/10 cm plate allowing 60% confluency in 24 hours. For the SIRM experiments, A549 cell media were changed to complete DMEM with glucose replaced by $^{13}C_6$-glucose (0.2% w/v) or with the addition of $^{13}C_1$-CH_3-methionine (0.2 mM). The cells were also grown in parallel using unlabeled media. For the experiment on treatment with seleno compounds, A549 or H1299 cell media were changed to vehicle (Ctl), 5 μM methylseleninic acid (MSA), 6.25 μM selenite (SeO_3), or 0.5 mM selenomethionine (SeM), which are the IC_{50} concentrations for A549 cells under these conditions ([34, 35] and unpublished data). The MSA medium was renewed after 12 h of treatment due to rapid metabolic degradation. After 24 hours, cells were quenched, polar metabolites extracted as described previously [36]. One eighteenth of the polar extracts lyophilized, dissolved in 0.5 mL 20 mM ammonium acetate (pH 7.4), and processed through PBA columns as described below.

2.3. Mouse liver extraction

Flash-frozen mouse liver tissues were pulverized under liq. N_2 and ca. 6–8 mg by wet weight was extracted for polar metabolites, as previously described [37]. One eighth of the polar extracts was lyophilized and dissolved in 0.5 mL 20 mM ammonium acetate for processing through PBA columns as described below.

The procedure to simultaneously quench, lyse, and extract polar metabolites from cells and tissues was as previously reported [38]. Briefly, the metabolism of cells or tissues was quenched and cell lysed with 1 mL of cold CH_3CN (stored at −20°C) before 0.75 mL of Nanopure water and 1 mL of cold $CHCl_3$ was added in a final $CH_3CN:H_2O:CHCl_3$ ratio of 2:1.5:1 (v/v). The polar, non-polar, and insoluble proteinaceous fractions were recovered. The polar fraction was aliquoted, lyophilized, and stored at −80 °C before processing for SAM/SAH analysis. The protein fraction was solubilized in 62.5 mM Tris + 2% SDS + 1 mM dithiothreitol (pH 6.8) for protein determination using the BCA method (Pierce Chemicals).

2.4. Human plasma sample collection and preparation

Blood was collected into a purple top vacutainer containing K_2-EDTA from two healthy volunteers (UK094, female and UK168, male) and a patient with (JK016) with intraductal papillary mucinous neoplasms (IPMN) according to approved IRB protocols (IRB #43807 and 48495). Blood samples were placed on ice immediately after collection, centrifuged within 30 min of collection at 3,500×g for 15 min at 4°C as described previously [39]. The plasma was then immediately acidified with 9 μL of 5 M acetic [26] or 4.5 μL formic acid per mL of plasma to stabilize SAM (final pH =4.5–5). Acidified plasmas were frozen in liquid N_2 and kept at −80°C. For extracting SAM and SAH, 10 μL of $^2H_3$-SAM (0.115 μM) and $^2H_4$-SAH (0.167 μM) was added to the thawed acidified plasma before neutralization to pH 7–7.5 with 1 M NH_4OH and 225–490 μL of which was immediately processed with PBA columns as described below.

2.5 PBA based-solid phase extraction for SAM and SAH

Bond-Elut PBA columns were used to capture SAM and SAH from polar extracts. The column was custom-made to have low sorbent mass (50 mg) in a 1 mL column to reduce the elution volume. Binding and elution were carried out essentially as described previously [24, 26, 40], but with the following modifications. The PBA column was acidified with 0.1 M formic acid (1 mL) before conditioning with 20 mM ammonium acetate (pH 7.4) solution (1 mL, 2 times). Plasma as is or reconstituted polar extract in 0.5 mL 20 mM ammonium acetate was applied to the conditioned column. The column was washed with 1 mL of 20 mM ammonium acetate for cell/tissue extracts or 2×1 mL of ammonium acetate for plasma samples to remove salts. Bound analytes were eluted using 200 μL of 0.1 M formic acid, which was repeated five times using the same eluate to result in a final collected volume of ca 200 μL. $^2H_4$-SAH (16.7 nM) and $^2H_3$-SAM (11.5 nM) were added to final eluates of cell/tissue extracts before dilution 1:1 with methanol containing 0.25 % formic acid (v/v) for DI-nESI-UHR-FTMS analysis. Eluates of plasma samples were lyophilized, resuspended in 15 μL of water and 10 μL of which was diluted to 50 μL with methanol + 0.25 % formic acid for DI-nESI-UHR-FTMS analysis. The final concentration for $^2H_4$-SAH and $^2H_3$-SAM in the spray solution was 22.3 and 15.4 nM, respectively.

2.6 DI-nESI-UHR-FTMS analysis of SAM/SAH and data processing

Samples were introduced using the nanoelectrospray TriVersa NanoMate (Advion Biosciences, Ithaca, NY, USA) with +1.45 kV electrospray voltage and 0.6 psi head pressure. UHR-FTMS data were collected on an Orbitrap Fusion Lumos Tribrid mass spectrometer (Lumos) from Thermo Scientific (San Jose, CA, USA) with 1,000,000 resolving power (at 200 m/z) in positive ion mode. Three different scan modes were used for data collection. MS^1 full scans were acquired using 2 microscans per scan in the m/z range of 150 to 1000; SIM scans were obtained to include m/z 399.1445 for SAM ($C_{15}H_{22}N_6O_5S$, $[M+H]^+$) and m/z 385.1289 for SAH ($C_{14}H_{20}N_6O_5S$, $[M+H]^+$) with 25 m/z isolation windows and 1 microscan per scan. Spectra were acquired over a continuous infusion period of 5–10 minutes, and spectra that exceeded a threshold were averaged. This process increased both signal to noise ratio and the mass accuracy, while removing low intensity scans that could impact quantification using peak area (ion intensity). The absolute

quantification was achieved by referencing to the ion intensity of internal deuterated standards.

The SIM m/z windows were chosen to accommodate all possible ^{13}C isotopologues. The MS^2 scans were collected via quadrupole isolation using 0.5 m/z isolation window and HCD (High Energy Collision Dissociation) set at 30 % collision energy with 100,000 or 500,000 resolving power to confirm standards and isotope labeled SAM and SAH. The AGC target was 10^5 with a maximal 1000 ms injection time for both MS^1 and MS^2 scans. The data collection time for MS^1 and MS^2 scans was 10 and 3 minutes, respectively.

The linearity of SAM/SAH analysis was performed by diluting a 10 μM standard mixture to concentrations ranging from 25 to 1000 nM using 50% methanol containing 0.1% formic acid. The UHR-FTMS analysis for each standard sample was repeated three times to check for precision.

Limits of detection were assessed by the apparent signal to noise ratio at the accurate mass with 1 ppm mass error for SAM and SAH, using a value of 5X above background noise (for detection) and 10X for the limit of quantification.

For data processing, the exact (accurate mass) m/z values and peak intensities were exported as an Excel file. Then, isotopologues of SAM and SAH were assigned using an in-house software PREMISE (PRecalculated Exact Mass Isotopologue Search Engine) [41] by matching theoretical m/z values against detected m/z values. The raw, observed m/z value was compared to the theoretical m/z values of SAM and SAH within a 0.002 m/z window for assignment; when internal standards were used, the resulting m/z correction resulted in a 0.001 m/z window- matching criterion. The peak intensity of all assigned isotopologues was corrected for natural abundance [42] to determine isotopic enrichment.

2.7 Ion chromatography-UHR-FTMS

Polar fractions of A549 cells were concentrated by nitrogen flushing using Evaporex® microplate evaporators (Apricot Designs, Covina, CA, USA). Typically 10% of total polar extracts (ca. 150 μL) were placed in the wells of 96-well plates and evaporated by continuous nitrogen flow (45 L min^{-1}) at 40 °C for 20 minutes, which concentrated the analytes by 3–4 fold. The concentrates were the analyzed as previously described [36] by IC-UHR-FTMS using a Dionex ICS-5000+ ion chromatograph connected to an Orbitrap Fusion Tribrid mass spectrometer (ThermoFisher) operated in negative ion mode. A Dionex IonPac AG11-HC-4 μm reagent-free ion chromatography and high pressure ion chromatography guard column (2 × 50 mm) was connected prior to anionic Dionex IonPac AC11-HC 4 μm RFIC&HPIC (2 × 250 mm) column. The mass resolution was set to 500,000 (FWHM at m/z 200). Peak areas and ^{13}C isotopologues of metabolites were determined using TraceFinder 3.3 (Thermo) and were corrected for natural abundance distribution for each isotopologue [36].

3.   Results & Discussion

3.1   DI-nESI-UHR-FTMS analysis of SAM and SAH standards

Figure 2a shows UHR mass spectra of standard SAH, SAM and the deuterium-labeled standards recorded with 10 min of signal averaging at a mass resolution of 1 million (at 200.0 m/z). The theoretical m/z values of proton adducts of SAH and SAM are 385.12887 and 399.14451 and in this case the observed m/z values were 385.12867 and 399.14427 respectively. The mass error of both SAM and SAH ions was 0.6 ppm, which was the same mass error for the $^2H_3$-SAM and $^2H_4$-SAH standards (Table 1). These deuterated external standards were well-resolved from the ^{13}C isotopologues of SAM and SAH in A549 cell extracts that had the same number of ^{13}C as that of ^2H atoms (Fig. 3a and b), which make them suitable for use in quantification for SIRM studies. In addition, as the resolution of FTMS was increased from 120,000 to 10^6 (Fig. S1), the natural abundance M+1 ^{13}C isotope of SAM (m/z=400.14691) was progressively separated from other unknown peaks. These data showed that it is crucially important to use UHR-FTMS to quantify labeled metabolites from crude extracts, including sample introduction via direct infusion. To confirm the structures and define the fragmentation patterns that are important for isotopomer analysis in SIRM experiments (see below), MS^2 spectra of each standard were analyzed at 120,000 resolution with 30% HCD and shown in Fig. 2b and c for SAH (385.1287 m/z) and $^2H_4$-SAH (389.1537 m/z), respectively. Several major fragment ions showed 4 Da differences between unlabeled and labeled SAH but the 136.06 m/z fragment ion did not, which corresponds to the adenine group released by cleavage at the glycosyl bond. Fig. S2a and b shows the MS^2 spectra of SAM (399.1443 m/z) and its $^2H_3$ standard (402.1631 m/z). Unlike the fragmentation patterns for SAH, only one minor fragment ion showed 3 m/z differences between SAM (298.10) and $^2H_3$-SAM (301.11) as the major fragment ions did not contain the C^2H_3 group.

We also determined the linear range of the MS response for SAM and SAH standards for optimizing of the SIRM analysis. As shown in Table S1 and Fig. S3, both SAM and SAH showed a good linear and reproducible response over the range of 25 to 1000 nM. The detection limit was somewhat better than published LC/MS methods [22, 43], illustrating the high sensitivity of UHR-FTMS along with its higher sample throughput. Together with the low coefficient of variation, this new method enabled rapid and reliable quantification of SAM and SAH.

3.2   Optimization of extraction conditions for A549 cells

It is crucially important to minimize the salt content in polar biological extracts to maintain stable electrospray ionization using direct infusion MS [28]. We took two simple measures to reduce the salt content in A549 cell extracts for SAM and SAH analysis. One is to perform a quick Nanopure water rinse of the cell culture before extraction. The other is to capture SAM and SAH by a PBA column via interaction of SAM/SAH's vicinal cis-diol group with PBA at neutral pH, followed by wash with ammonium acetate, elution with volatile formic acid, and lyophilization to remove formic acid. Similar PBA cleanup methods have been used by other researchers for SAM and SAH analysis [24, 26, 40]. We

found that the electrospray ionization stability was significantly improved with this desalting approach (data not shown).

As SAM has been reported to be unstable at pH above 6.0 [44], the effect of pH on cell lysis and extraction was also evaluated. Simultaneous cell lysis and extraction was performed in aqueous 60% CH_3CN containing 18 MOhm deionized water, 0.01 M formic acid, and 0.1 M formic acid. The pH of the final extracts were 6.0, 5.0, and 3.5 respectively. Fig. S4a to c show the MS^1 spectra of SAM from these polar extracts of A549 cells, which showed the lowest MS intensity for the extract at pH 3.5. We have also performed lysis and extraction at pH 1.5 by adding 0.05 M HCl, but the MS intensity of SAM was no higher than that at pH 5 (data not shown). Although the SAM stability is known to be greater in acidic conditions than at neutral pH, we found that moderately acidic conditions (pH 5.0 to 6.0) for recovering SAM from A549 cell were better suited for DI-nESI-UHR-FTMS analysis. SAH also displayed the lowest MS intensity at pH 3.5, followed by pH 5.0 and 6.0 (Fig. S4). There appeared to be some advantage to extraction at pH 5.0 for SAM analysis but the number of metabolites analyzable by IC-UHR-FTMS was lower at pH 5 than at pH 6 (see below). Using the external standards, we determined recoveries of 93± 4% for SAH and 91± 2.5% for SAM at pH 6.

Our goal is to have a lysis/extraction method that not only reliably recovers SAM and SAH but also many other metabolites in SIRM experiments. We analyzed the A549 extracts at the three different pH's by IC-UHR-FTMS to determine the number of assignable metabolites. Table S2 lists the peak areas of metabolites detected in the negative ion mode. The number of negatively charged metabolites was highest for pH 6 (123), followed by pH 5 (117) and pH 3.5 (78) extractions, due at least in part to the instability of some metabolites (e.g. ATP, fructose-1,6-bisphosphate) at lower pH values. Thus, 60% CH_3CN in Nanopure water (pH 6) was chosen for recovering SAM/SAH from biological systems (except for plasma) for DI-nESI-UHR-FTMS analysis. It should be noted that this lysis/extraction method has been used by us in most of our SIRM studies [28, 45, 46].

In addition to SAM and SAH, other metabolites that contain vicinal hydroxyls are expected to be retained on the PBA column. Table S2 shows a total of 35 such quantifiable analytes in the pH 6 eluate of the PBA column including nucleotides (e.g. AMP) and several 2-hydroxy acids (e.g. 2-hydroxyglutarate).

3.3   Quantification of SAM and SAH in mouse liver tissue and human plasma

We applied the above optimized method to analyze SAM and SAH in mouse liver tissue extracts. Fig. 4a shows a MS^1 spectrum acquired over 4 minutes of infusion of a 1/8 fraction of polar extract from about 8 mg wet weight of mouse liver tissue. The MS intensity of SAM (3.1.5e3) and SAH (5.5e3) was higher than that of the spiked external standards and well-resolved from other unknown peaks in full scan mode (384–403 m/z shown). Note the extremely small deviation from theoretical m/z for uncorrected spectra, in each case < 0.0004 m/z. Repeated analyses showed the concentrations of SAM and SAH in the polar extract of this mouse liver tissue were 0.254 μM and 0.117 μM, respectively, which corresponded to 0.052 and 0.023 μmole g^{-1} protein and a SAM/SAH ratio of 2.3. The

recoveries determined by spiking of external standards were 89±1.5% for SAH and 89±6% for SAM.

For the human plasma samples (Figure 4b), both SAM and SAH were readily observed in the full scan mode spectrum. Here again, note the extremely small deviation from theoretical m/z for the uncorrected spectra, in each case < 0.0002 m/z. Table S3 lists the plasma concentrations of SAM and SAH for two healthy and one IPMN patient volunteers. Previous studies have reported the concentration of SAM and SAH in healthy human plasma to be in the nanomolar range (50 to 155 nM for SAM) using LC/MS or ELISA methods [26, 43, 47]. Our analysis showed that the SAM concentration of the healthy subjects was at the low end of the literature range while that of one IPMN patient was much above the range. Our analysis also showed that SAH was below detectable limits in the two healthy plasma samples and the SAM/SAH ratio for the IPMN patient was 71, which was much higher than the literature range for healthy adults (2.7–12.4) [26]. As SAH is an indicator of not only SAM metabolism but also a principal degradation product of SAM due to sample handling and processing, this lack of detectable SAH (i.e. below the sub nM detection limit) in our healthy plasma samples indicates very low SAM breakdown resulting from sample handling. Whether the abnormally high SAM concentration in the IPMN patient is representative of this disease awaits further investigation.

3.4   SAM/SAH synthesis from $^{13}C_6$ glucose and $^{13}CH_3$-methionine in A549 cells.

To demonstrate the method for tracking newly synthesized SAM and SAH in cell cultures, we incubated A549 cells for 24 hours in media containing $^{13}C_6$ glucose, $^{13}CH_3$-methionine, or the unlabeled counterparts. The average total abundances of SAM and SAH were determined to be about 1.5 and 0.35–0.5 μmol g^{-1} protein, respectively, with a SAM to SAH ratio of 2.9–4.5 (Table S4).

We also determined the fractional enrichment of different isotopologues of SAM, SAH, and ATP as well as their PPP precursors (analyzed by IC-UHR-FT-MS) with each tracer treatment and corrected for natural abundance [42] as shown in Fig. 5. With $^{13}C_6$-glucose as tracer (Fig. 5A), the most abundant ^{13}C isotopologues for the PPP metabolites were the uniformly ^{13}C labeled species (e.g. **5** or $^{13}C_5$-R5P in **c** and **7** or $^{13}C_7$-S7P in **d**), as expected from the atom-resolved pathway tracing. Also consistent with the pathway tracing was the significant presence of species such as $^{13}C_2$-/$^{13}C_5$-S7P and $^{13}C_4$-/$^{13}C_5$-F6P (**f**). $^{13}C_5$-R5P was then converted to $^{13}C_5$-PRPP (**g**) before incorporation into ATP (**h**), SAM (**i**), and SAH (**j**). Thus, the predominant **5** isotopologue in ATP/SAM/SAH is consistent with the high extent of $^{13}C_5$-ribose incorporation, which we have shown for ATP previously [48]. Less abundant isotopologues of the three metabolites but present significantly were the $^{13}C_6$- (**6**) and $^{13}C_7$- (**7**) species, which represents $^{13}C_1$- and $^{13}C_2$-adenine (generated via one-carbon metabolism) plus $^{13}C_5$-ribose. This ^{13}C labeling pattern of ATP in $^{13}C_6$-glucose-grown A549 cells recapitulated that in our previous study [28]. In SAM, the higher ratio for the fractional enrichment of the $^{13}C_6$- (**6**) over $^{13}C_7$- (**7**) isotopologue than that in ATP (Fig. 5B) could be accounted for by the contribution of the $^{13}CH_3 + ^{13}C_5$-ribose (in addition to the $^{13}C_1$-adenine + $^{13}C_5$-ribose) species to the **6** isotopologue in SAM.

In comparison, with $^{13}CH_3$-methionine as tracer, SAM (**a**) but not SAH (**b**) showed significant $^{13}C_1$ labeling, i.e. ca. 50% in fractional enrichment (Fig. 5C), which was comparable to that of methionine supplied in the medium. This indicates an efficient conversion of exogenous methionine to SAM presumably via the action of methionine adenosyltransferase (MAT) and loss of the $^{13}CH_3$ group in SAH via the action of methyltransferases in A549 cells.

To confirm the position of incorporated ^{13}C in SAM and SAH, we acquired and analyzed the MS/MS patterns of m0, m1, and m5 ions of SAM. Fig. 6a shows the tandem mass spectrum of the m0 ion. The three most abundant ions at m/z 250.09, 136.06, and 102.06 corresponded respectively to (i) the product of cleavage at the S-methionine to C5-ribose bond to release adenosine, (ii) that at the N9-adenine to C1-ribose bond to release adenine and (iii) that at the S to C4 bond of methionine to release 2-aminobutanoate. The other product ions at m/z 150.05, 264.09, and 298.10, have relatively lower intensities. In the tandem mass spectrum of m1 SAM (Fig. 6b), the m/z values of fragment ions containing the methyl-group of SAM were +1 m/z shifted (298.10->299.10, 150.05 ->151.05, and 264.09->265.09), which confirmed ^{13}C labeling at the methyl position of SAM with $^{13}C_1$-methionine as tracer. With $^{13}C_6$-glucose as tracer, the m5 ion of SAM in Fig. 6c yielded ribose-containing fragment ions that were +5 Da shifted (298.10 -> 303.10, 250.09 -> 255.11, and 264.09 -> 269.09). These data confirmed the m5 ion to arise from $^{13}C_5$-ribose of the adenosyl subunit of SAM. Thus, SAM and SAH analysis using the new method demonstrated efficient SAM synthesis from methionine and *de novo* synthesis of SAM/SAH from glucose in A549 cells.

3.5   Cell line-dependent perturbations of SAM/SAH levels and ratios by MSA, selenite, and SeM treatments

We further demonstrated the new method by analyzing the effect of three different anti-cancer selenium agents (MSA, SeO_3, and SeM) on SAM and SAH status in two lung adenocarcinoma (A549 and H1299) cell lines. Figure 7a shows the depleting effect of the three agents on SAM and SAH levels in A549 cells, which was similarly observed in H1299 cells except for the SeO_3 treatment (Fig. 7c). This effect could result from decreased synthesis and/or increased utilization of SAM and SAH. However, SAM depletion without the buildup of the product SAH is more consistent with a block in SAM synthesis, which is corroborated by the attenuating effect of SeO_3 [34] and MSA [49] on the synthesis of SAM's precursor, ATP in A549 cells. In contrast, the SAM to SAH ratio was unaltered in all but one case, i.e. it more than doubled in MSA- versus in control-treated A549 cells (Fig. 7b, d). This increase in SAM to SAH ratio despite the depletion of SAM levels in A549 cells points to an inhibition of the methyltransferases that catalyze DNA/RNA/protein methylation (cf. Fig. 1), besides the block in SAM synthesis. In addition, the buildup of SAM with the lack of change in SAM to SAH ratio in SeO_3-treated H1299 cells (Fig. 7c, d) suggests activation of SAM synthesis. Pending further confirmation, the SAM/SAH analysis using our new method revealed cell line- and Se form-dependence in perturbing one-carbon metabolism in lung cancer cells.

4. Conclusions

We have developed a rapid, sensitive, and robust method for SAM and SAH analysis in biological extracts by coupling PBA affinity capture with DI-nESI-UHR-FTMS, that supports metabolic tracing using ^{13}C (SIRM). As the lysis/extraction solvent system (CH_3CN in mildly acidic Nanopore water) used to efficiently recovered SAM/SAH was the same as that for extracting polar metabolites in general, this method is compatible with comprehensive metabolite profiling studies including SIRM applications. This is an added advantage over the existing methods that call for extensive sample acidification, which leads to degradation of acid-labile metabolites. In addition, harnessing UHR-FTMS to resolve the same number of ^{13}C from ^2H labels in SAM and SAH enabled the use of ^2H-labeled external standards for reliable quantification of SAM/SAH in complex biological matrices including those containing ^{13}C labeled metabolites. We first demonstrated the utility of the method on SAM/SAH quantification in mouse liver, A549 cells, and human plasma samples. Then, we applied the method to track ^{13}C incorporation from $^{13}C_1$-methionine and $^{13}C_6$-glucose into SAM and SAH in A549 cells via the MAT activity and the PPP-purine nucleotide synthesis pathway, respectively. Moreover, we used the method to discover that MSA may block both SAM synthesis and its use in methylation reactions. Thus, the new method is applicable to both high throuput and tracer-based metabolic pathway analysis for SAM and SAH, thereby facilitating the understanding of epigenetic metabolism and regulation.

Supplementary Material

Refer to Web version on PubMed Central for supplementary material.

Acknowledgments.

Abbreviations:

DI-nESI-UHR-FTMS	direct infusion nanoelectrospray ultra-high-resolution Fourier transform mass spectrometry
DMEM	Dulbecco's modified Eagle's medium
ESI	electrospray ionization
MSA	methylseleninic acid
PBA	phenylboronic acid
SeO$_3$	selenite

SAH	S-adenosylhomocysteine
SAM	S-adenosylmethionine
SeM	selenomethionine
SIRM	stable isotope-resolved metabolomics
THF	tetrahydrofolate

References

[1]. Sanderson SM, Gao X, Dai Z, Locasale JW, Methionine metabolism in health and cancer: a nexus of diet and precision medicine, Nat Rev Cancer, 19 (2019) 625–637. [PubMed: 31515518]

[2]. Locasale JW, Serine, glycine and one-carbon units: cancer metabolism in full circle, Nat Rev Cancer, 13 (2013) 572–583. [PubMed: 23822983]

[3]. Finkelstein JD, Methionine metabolism in mammals, J Nutr Biochem, 1 (1990) 228–237. [PubMed: 15539209]

[4]. Newman AC, Maddocks ODK, One-carbon metabolism in cancer, Br J Cancer, 116 (2017) 1499–1504. [PubMed: 28472819]

[5]. Ducker GS, Rabinowitz JD, One-Carbon Metabolism in Health and Disease, Cell Metab, 25 (2017) 27–42. [PubMed: 27641100]

[6]. Lu SC, Mato JM, S-adenosylmethionine in liver health, injury, and cancer, Physiol Rev, 92 (2012) 1515–1542. [PubMed: 23073625]

[7]. Zhang J, Zheng YG, SAM/SAH Analogs as Versatile Tools for SAM-Dependent Methyltransferases, ACS Chem Biol, 11 (2016) 583–597. [PubMed: 26540123]

[8]. Mudd SH, Brosnan JT, Brosnan ME, Jacobs RL, Stabler SP, Allen RH, Vance DE, Wagner C, Methyl balance and transmethylation fluxes in humans, Am J Clin Nutr, 85 (2007) 19–25. [PubMed: 17209172]

[9]. Green TJ, Skeaff CM, McMahon JA, Venn BJ, Williams SM, Devlin AM, Innis SM, Homocysteine-lowering vitamins do not lower plasma S-adenosylhomocysteine in older people with elevated homocysteine concentrations, Br J Nutr, 103 (2010) 1629–1634. [PubMed: 20089204]

[10]. Zhang H, Liu Z, Ma S, Zhang H, Kong F, He Y, Yang X, Wang Y, Xu H, Yang A, Tian J, Zhang M, Cao J, Jiang Y, Guo X, Ratio of S-adenosylmethionine to S-adenosylhomocysteine as a sensitive indicator of atherosclerosis, Mol Med Rep, 14 (2016) 289–300. [PubMed: 27175774]

[11]. Mato JM, Corrales FJ, Lu SC, Avila MA, S-Adenosylmethionine: a control switch that regulates liver function, FASEB J, 16 (2002) 15–26. [PubMed: 11772932]

[12]. Elshorbagy AK, Jerneren F, Samocha-Bonet D, Refsum H, Heilbronn LK, Serum S-adenosylmethionine, but not methionine, increases in response to overfeeding in humans, Nutr Diabetes, 6 (2016) e192. [PubMed: 26807510]

[13]. Mentch SJ, Mehrmohamadi M, Huang L, Liu X, Gupta D, Mattocks D, Gomez Padilla P, Ables G, Bamman MM, Thalacker-Mercer AE, Nichenametla SN, Locasale JW, Histone Methylation Dynamics and Gene Regulation Occur through the Sensing of One-Carbon Metabolism, Cell Metab, 22 (2015) 861–873. [PubMed: 26411344]

[14]. Pizzolo F, Blom HJ, Choi SW, Girelli D, Guarini P, Martinelli N, Stanzial AM, Corrocher R, Olivieri O, Friso S, Folic acid effects on s-adenosylmethionine, s-adenosylhomocysteine, and DNA methylation in patients with intermediate hyperhomocysteinemia, J Am Coll Nutr, 30 (2011) 11–18. [PubMed: 21697534]

[15]. Tran TQ, Lowman XH, Kong M, Molecular Pathways: Metabolic Control of Histone Methylation and Gene Expression in Cancer, Clin Cancer Res, 23 (2017) 4004–4009. [PubMed: 28404599]

[16]. Mato JM, Martinez-Chantar ML, Lu SC, S-adenosylmethionine metabolism and liver disease, Ann Hepatol, 12 (2013) 183–189. [PubMed: 23396728]

[17]. Kruglova MP, Grachev SV, Bulgakova PO, Ivanov AV, Virus ED, Nikiforova KA, Fedoseev AN, Savina GD, Kubatiev AA, Low S-adenosylmethionine/ S-adenosylhomocysteine Ratio in Urine is Associated with Chronic Kidney Disease, Lab Med, 51 (2020) 80–85. [PubMed: 31247080]

[18]. Mato JM, Alvarez L, Ortiz P, Pajares MA, S-adenosylmethionine synthesis: molecular mechanisms and clinical implications, Pharmacol Ther, 73 (1997) 265–280. [PubMed: 9175157]

[19]. Hanson NQ, Eckfeldt JH, Schwichtenberg K, Aras O, Tsai MY, Interlaboratory variation of plasma total homocysteine measurements: results of three successive homocysteine proficiency testing surveys, Clin Chem, 48 (2002) 1539–1545. [PubMed: 12194931]

[20]. O'Broin SD, Kelleher BP, McPartlin J, O'Gorman P, Browne M, White B, Smith OP, Optimization of routine plasma homocysteine monitoring, Blood Coagul Fibrinolysis, 11 (2000) 367–369. [PubMed: 10847424]

[21]. Melnyk S, Pogribna M, Pogribny IP, Yi P, James SJ, Measurement of plasma and intracellular S-adenosylmethionine and S-adenosylhomocysteine utilizing coulometric electrochemical detection: alterations with plasma homocysteine and pyridoxal 5'-phosphate concentrations, Clinical chemistry, 46 (2000) 265–272. [PubMed: 10657384]

[22]. Guiraud SP, Montoliu I, Da Silva L, Dayon L, Galindo AN, Corthesy J, Kussmann M, Martin FP, High-throughput and simultaneous quantitative analysis of homocysteine-methionine cycle metabolites and co-factors in blood plasma and cerebrospinal fluid by isotope dilution LC-MS/MS, Anal Bioanal Chem, 409 (2017) 295–305. [PubMed: 27757515]

[23]. Struys EA, Jansen EE, de Meer K, Jakobs C, Determination of S-adenosylmethionine and S-adenosylhomocysteine in plasma and cerebrospinal fluid by stable-isotope dilution tandem mass spectrometry, Clin Chem, 46 (2000) 1650–1656. [PubMed: 11017945]

[24]. Kirsch SH, Knapp JP, Geisel J, Herrmann W, Obeid R, Simultaneous quantification of S-adenosyl methionine and S-adenosyl homocysteine in human plasma by stable-isotope dilution ultra performance liquid chromatography tandem mass spectrometry, J Chromatogr B Analyt Technol Biomed Life Sci, 877 (2009) 3865–3870.

[25]. Jiang Z, Liang Q, Luo G, Hu P, Li P, Wang Y, HPLC-electrospray tandem mass spectrometry for simultaneous quantitation of eight plasma aminothiols: application to studies of diabetic nephropathy, Talanta, 77 (2009) 1279–1284. [PubMed: 19084635]

[26]. Gellekink H, van Oppenraaij-Emmerzaal D, van Rooij A, Struys EA, den Heijer M, Blom HJ, Stable-isotope dilution liquid chromatography-electrospray injection tandem mass spectrometry method for fast, selective measurement of S-adenosylmethionine and S-adenosylhomocysteine in plasma, Clinical chemistry, 51 (2005) 1487–1492. [PubMed: 15919880]

[27]. Lane AN, Fan TW, Higashi RM, Tan J, Bousamra M, Miller DM, Prospects for clinical cancer metabolomics using stable isotope tracers, Exp Mol Pathol, 86 (2009) 165–173. [PubMed: 19454273]

[28]. Lorkiewicz P, Higashi RM, Lane AN, Fan TW, High information throughput analysis of nucleotides and their isotopically enriched isotopologues by direct-infusion FTICR-MS, Metabolomics, 8 (2012) 930–939. [PubMed: 23101002]

[29]. Bruntz RC, Lane AN, Higashi RM, Fan TW, Exploring cancer metabolism using stable isotope-resolved metabolomics (SIRM), The Journal of biological chemistry, 292 (2017) 11601–11609. [PubMed: 28592486]

[30]. Fan TW, Lorkiewicz PK, Sellers K, Moseley HN, Higashi RM, Lane AN, Stable isotope-resolved metabolomics and applications for drug development, Pharmacol Ther, 133 (2012) 366–391. [PubMed: 22212615]

[31]. Lane AN, Fan TW, Bousamra M 2nd, Higashi RM, Yan J, Miller DM, Stable isotope-resolved metabolomics (SIRM) in cancer research with clinical application to nonsmall cell lung cancer, OMICS, 15 (2011) 173–182. [PubMed: 21329461]

[32]. Yang Y, Fan TW, Lane AN, Higashi RM, Quantification of Isotopologues of Amino Acids by Multiplexed Stable Isotope-Resolved Metabolomics Using Ultrahigh-Resolution Mass Spectrometry Coupled with Direct Infusion, in: Alterman M (Ed.) Amino Acid analysis, Humana, New York, NY, 2019, pp. 57–68.

[33]. Maegley KA, Krivacic C, Bingham P, Liu W, Brooun A, Comparison of a High-Throughput Mass Spectrometry Method and Radioactive Filter Binding to Assay the Protein Methyltransferase PRMT5, Assay Drug Dev Technol, 13 (2015) 235–240. [PubMed: 26065559]

[34]. Fan T, Bandura L, Higashi R, Lane A, Metabolomics-edited transcriptomics analysis of Se anticancer action in human lung cancer cells, Metabolomics, 1 (2005) 325–339

[35]. Fan TW-M, Tan JL, McKinney MM, Lane AN, Stable Isotope Resolved Metabolomics Analysis of Ribonucleotide and RNA Metabolism in Human Lung Cancer Cells., Metabolomics, 8 (2012) 517–527. [PubMed: 26146495]

[36]. Sun Q, Fan TW-M, Lane AN, Higashi RM, Ion Chromatography-Ultra High-resolution MS1/MS2 Method for Stable Isotope-Resolved Metabolomics (SIRM) Reconstruction of Metabolic Networks., Anal. Chem, 93 (2021) 2749–2757. [PubMed: 33482055]

[37]. Sun RC, Fan TWM, Deng P, Higashi RM, Lane AN, Le A-T, Scott TL, Sun Q, Warmoes MO, Yang Y, Noninvasive liquid diet delivery of stable isotopes into mouse models for deep metabolic network tracing, Nature communications, 8 (2017) 1646.

[38]. Fan TW-M, Sample preparation for metabolomics investigation, in: Fan TW-M, Lane AN, Higashi RM (Eds.) The Handbook of Metabolomics: Pathway and Flux Analysis, Methods in Pharmacology and Toxicology, Springer Science, New York, 2012, pp. 7–27.

[39]. Fan TWM, Zhang X, Wang C, Yang Y, Kang W-Y, Arnold S, Higashi RM, Liu J, Lane AN, Exosomal lipids for classifying early and late stage non-small cell lung cancer, Analytica chimica acta, 1037 (2018) 256–264. [PubMed: 30292300]

[40]. Iglesias Gonzalez T, Cinti M, Montes-Bayon M, Fernandez de la Campa MR, Blanco-Gonzalez E, Reversed phase and cation exchange liquid chromatography with spectrophotometric and elemental/molecular mass spectrometric detection for S-adenosyl methionine/S-adenosyl homocysteine ratios as methylation index in cell cultures of ovarian cancer, J Chromatogr A, 1393 (2015) 89–95. [PubMed: 25836049]

[41]. Lane AN, Fan TW, Xie Z, Moseley HN, Higashi RM, Isotopomer analysis of lipid biosynthesis by high resolution mass spectrometry and NMR, Anal Chim Acta, 651 (2009) 201–208. [PubMed: 19782812]

[42]. Moseley HN, Correcting for the effects of natural abundance in stable isotope resolved metabolomics experiments involving ultra-high resolution mass spectrometry, BMC Bioinformatics, 11 (2010) 139. [PubMed: 20236542]

[43]. Krijt J, Duta A, Kozich V, Determination of S-Adenosylmethionine and S-Adenosylhomocysteine by LC-MS/MS and evaluation of their stability in mice tissues, J Chromatogr B Analyt Technol Biomed Life Sci, 877 (2009) 2061–2066.

[44]. Hoffman JL, Chromatographic analysis of the chiral and covalent instability of S-adenosyl-L-methionine, Biochemistry, 25 (1986) 4444–4449. [PubMed: 3530324]

[45]. Sengupta D, Cassel T, Teng KY, Aljuhani M, Chowdhary VK, Hu P, Zhang X, Fan TW, Ghoshal K, Regulation of hepatic glutamine metabolism by miR-122, Molecular metabolism, 34 (2020) 174–186. [PubMed: 32180557]

[46]. Sun Q, Fan TWM, Lane AN, Higashi RM, Applications of chromatography-ultra high-resolution MS for stable isotope-resolved metabolomics (SIRM) reconstruction of metabolic networks, TrAC Trends in Analytical Chemistry, 123 (2020) 115676. [PubMed: 32483395]

[47]. Caudill MA, Wang JC, Melnyk S, Pogribny IP, Jernigan S, Collins MD, Santos-Guzman J, Swendseid ME, Cogger EA, James SJ, Intracellular S-adenosylhomocysteine concentrations predict global DNA hypomethylation in tissues of methyl-deficient cystathionine beta-synthase heterozygous mice, J Nutr, 131 (2001) 2811–2818. [PubMed: 11694601]

[48]. Sun Q, Fan TWM, Lane AN, Higashi RM, An Ion Chromatography–Ultrahigh-Resolution-MS1/Data-Independent High-Resolution MS2 Method for Stable Isotope-Resolved Metabolomics Reconstruction of Central Metabolic Networks, Analytical Chemistry, 93 (2021) 2749–2757 [PubMed: 33482055]

[49]. Tarrado-Castellarnau M, Cortés R, Zanuy M, Tarragó-Celada J, Polat IH, Hill R, Fan TWM, Link W, Cascante M, Methylseleninic acid promotes antitumour effects via nuclear FOXO3a translocation through Akt inhibition, Pharmacological Research, 102 (2015) 218–234. [PubMed: 26375988]
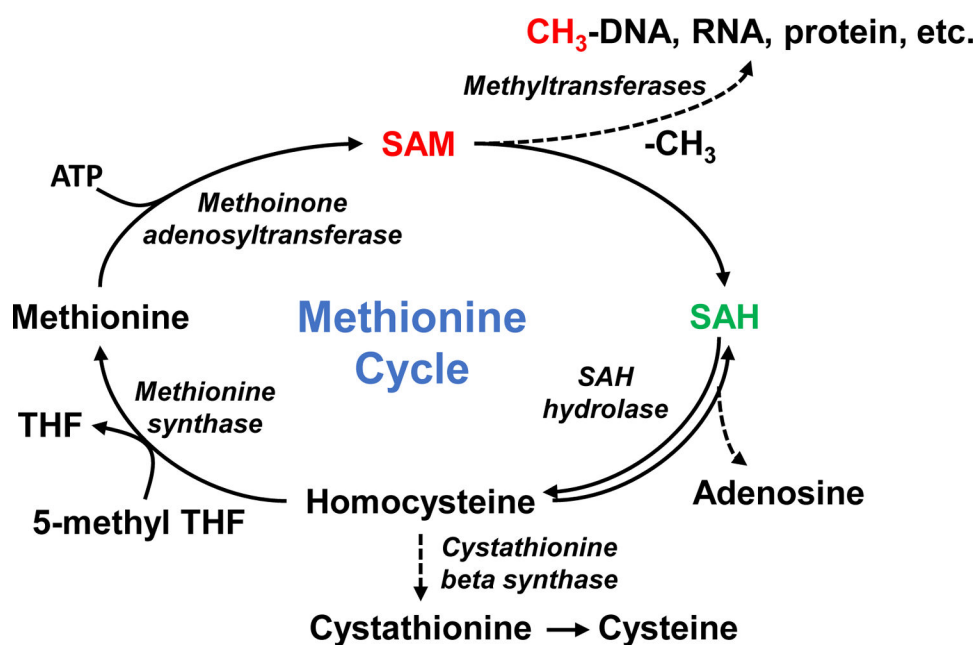
Figure 1. Inter-conversion of SAM and SAH in the transmethylation cycle.
SAM, S-adenosylmethionine; SAH, S-adenosylhomocysteine; THF, tetrahydrofolate; 5-methyl THF, 5-methyltetrahydrofolate.
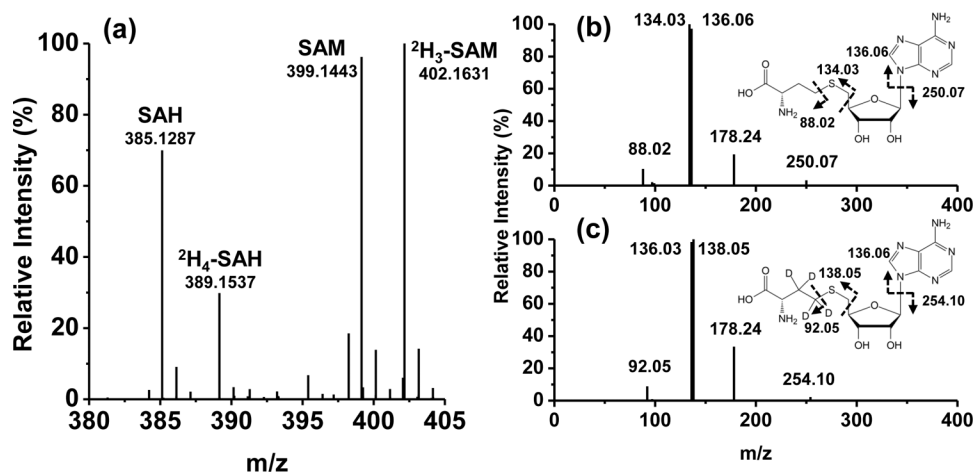
Figure 2. Ultrahigh resolution mass spectra of SAM and SAH

Standards and deuterated versions were prepared and introduced into the Orbitrap as described in Experimental. a) MS spectrum of S-adenosylmethionine (SAM, 399.1443 m/z), S-adenosylhomocysteine (SAH, 385.1287 m/z), $^2H_3$-labeled SAM (402.1631 m/z), and $^2H_4$-labeled SAH (389.1537 m/z) standards; b) MS^2 spectrum and structure of SAH with bond cleavages and resulting mass fragments; c) MS^2 spectrum of $^2H_4$-labeled SAH with bond cleavages and the resulting mass fragments.

Figure 3. MS spectra of ^{2}H standards of SAH and SAM added to A549 cell extracts containing ^{13}C-labeled SAH and SAM.

Sample preparation, experimental condirions and analyses were as as described in Experimental.
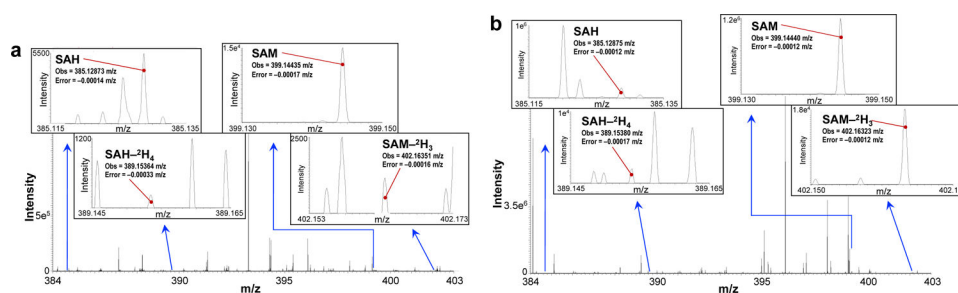
Figure 4. MS^1 spectra of SAM and SAH from mouse liver extract and human plasma, with internal standards SAM-^{2}H$_3$ and SAH-^{2}H$_4$.

Samples were prepared as described in the Experimental. **a**) Mouse liver extract spectrum comprising 69 FT spectra from over approx. 4 min acquisition under full scan MS^1 100–1000 m/z at 1M resolution setting and divided by the number of summed scans to provide an average. The averaged peak intensity or area is normalized to that of the internal deuterated standard to determine the concentration. The region displayed is 384 – 403 m/z and the insets show 0.02 m/z windows for greater detail. Errors stated are accurate mass errors from theoretical m/z values. **b**) Human plasma spectrum of a pancreatic cancer patient. The spectrum comprises 82 spectra averaged over approx. 9 min acquisition under full scan MS^1 150–1000 m/z at 1 M resolution setting. The averaged intensity is normalized to that of the internal deuterated standard to determine the concentration. The region displayed is 384 – 403 m/z and the insets show 0.02 m/z windows for greater detail. Errors stated are accurate mass deviation from theoretical m/z values.
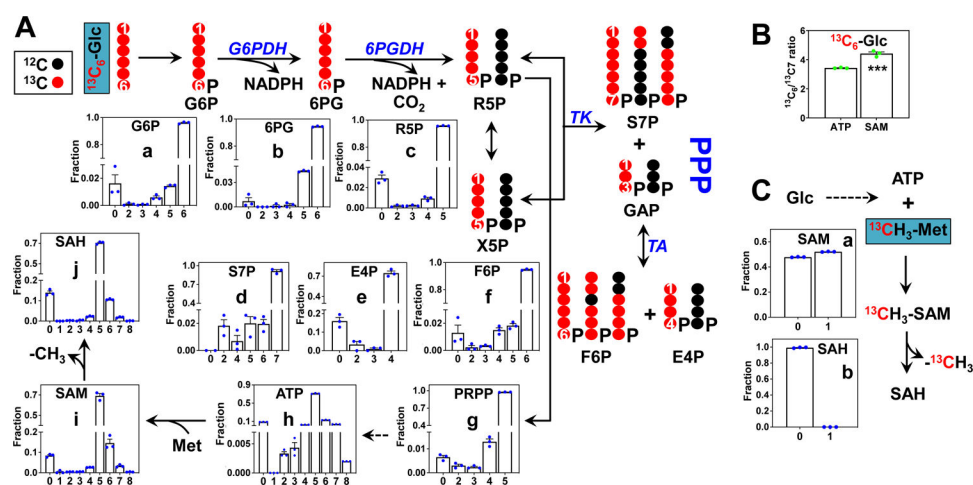
Figure 5. ^{13}C Isotopologue distributions of SAM, SAH and their precursors in A549 cells grown on ^{13}C$_6$-glucose or ^{13}CH$_3$-methionine

A549 cells were grown under standard conditions in media containing no ^{13}C-enriched tracers, ^{13}C$_6$-glucose (^{13}C$_6$-Glc) or ^{13}CH$_3$-methionine (^{13}CH$_3$-Met) as described in Experimental. The tracer experiments were done with n=3 and unlabeled experiment with n=2. Values on the X-axis denote the number of ^{13}C for each isotopologue. SAM and SAH were measured using the described method, and other metabolites were measured using the method described in ref 36.

a. Fractional distribution of metabolite isotopologues in the pentose phosphate pathway (PPP) and those of the downstream products phosphoribosyl pyrophosphate (PRPP), ATP, SAM, and SAH in ^{13}C$_6$-glucose grown samples. The atom tracing scheme depicts the more abundant isotopologue species resulting from the transformation of ^{13}C$_6$-Glc via the PPP. G6P: glucose-6-phosphate; 6PG: 6-phosphogluconate; R5P: ribose/ribulose-5-phosphate; X5P: xylulose-5-phosphate; S7P: sedoheptulose-7-phosphate; E4P: erythrose-4-phosphate; F6P: fructose-6-phosphate; G6PDH: glucose-6-phosphate dehydrogenase; 6PGDH: 6-phosphogluconate dehydrogenase; TK: transketolase; TA: transaldolase.

b. Ratio of the ^{13}C$_6$- to ^{13}C$_7$-isotopologues of ATP and SAM derived from ^{13}C$_6$-Glc. A higher ratio in SAM than that in ATP reflect ^{13}C labeling in the methyl group of SAM. ***: p-value 0.0012

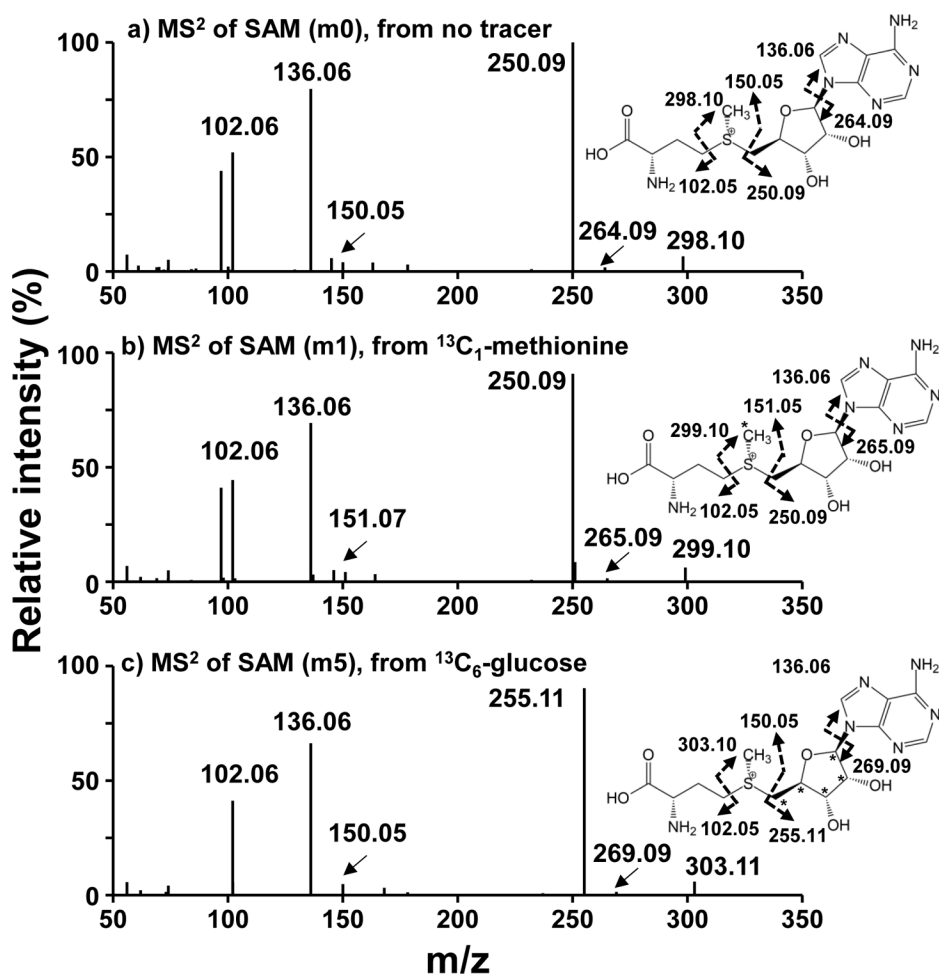c. Fractional distribution of isotopologues of SAM and SAH in ^{13}CH$_3$-Met grown samples.

Figure 6. MS/MS spectra of SAM from A549 cells exposed to $^{13}C_6$-glucose or $^{13}C_1$-CH$_3$-methionine

Cells were grown as described for Figure 5.

a. MS/MS of m0 isotopologue of SAM (399.1443 m/z) from an unlabeled sample

b. MS/MS of m1 isotopologue of SAM (400.1479 m/z) from a $^{13}C_1$-methionine labeled A549 cell extract,

c. MS/MS of m5 isotopologue of SAM (404.1613 m/z) from a $^{13}C_6$-glucose labeled A549 cell extract.

Data were acquired at a setting of 500 K mass resolution with 10 μscan/scan. Asterisks(*) represent ^{13}C.

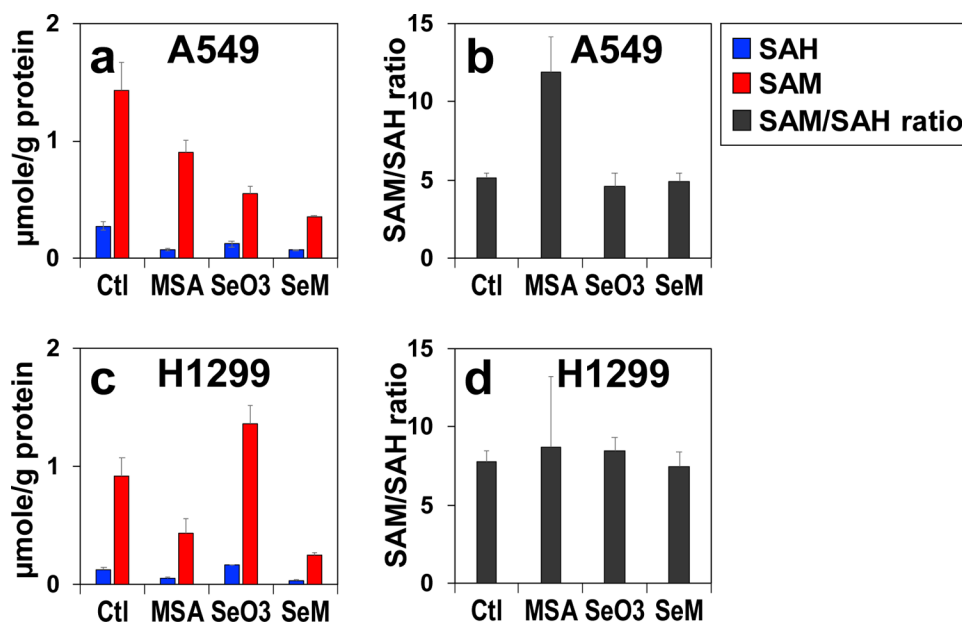Dashed arrows represent the fragmentation positions giving rise to the observed m/z.

Figure 7. Cell line-dependent perturbations of SAM/SAH levels and ratios by MSA, selenite, and SeM treatments.

A549 (a,b) and H1299 (a,b) cells were treated with 5 μM MSA, 6.25 μM selenite, or 0.5 mM SeM for 24 h (n = 3), extracted for polar metabolites, and analyzed for SAM/SAH as described in Experimental. ■: SAH; ■: SAM; ■: SAM/SAH ratio.

Table 1.

Chemical formula, theoretical and observed m/z ([M+H]$^+$) values, and mass error of SAM, SAH and their isotopically enriched standard in Fig. 2a.

	Formula	Theoretical mass (m/z), [M+H]$^+$	Observed mass (m/z), [M+H]$^+$	Mass error (ppm)
SAM	$C_{15}H_{22}N_6O_5S$	399.14451	399.14427	−0.6
D$_3$-SAM	$C_{15}H_{19}D_3N_6O_5S$	402.16335	402.16309	−0.6
SAH	$C_{14}H_{20}N_6O_5S$	385.12887	385.12862	−0.6
D$_4$-SAH	$C_{14}H_{16}D_4N_6O_5S$	389.15397	389.15372	−0.6